


Deterministic and stochastic coarsening control in optically addressed spatial light modulators subject to optical feedback

Vladimir V. Semenov ^{1,2,*} Xavier Porte,^{2,3} Laurent Larger,² and Daniel Brunner²

¹*Institute of Physics, Saratov State University, Astrakhanskaya Street 83, 410012 Saratov, Russia*

²*Optics Department, FEMTO-ST Institute, UMR CNRS 6174,*

University of Franche-Comté, 15B avenue des Montboucons, Besançon Cedex 25030, France

³*Institute of Photonics, Department of Physics, University of Strathclyde, 99 George Street, Glasgow G1 1RD, United Kingdom*



(Received 28 February 2023; accepted 7 July 2023; published 24 July 2023)

Phase separation accompanied by domain growth and coarsening is a phenomenon common to a broad variety of dynamical systems. In this context, controlling such processes represents a relevant interdisciplinary problem. Through numerical modeling, we demonstrate two complementary approaches of coarsening control in bistable systems based on the example of a spatially extended model describing an optically addressed spatial light modulator with two-color illumination subject to optical feedback. The first method implies varying system parameters such that the system evolves as the pitchfork or saddle-node normal forms. The second method leverages noise, whose intensity serves as an additional system control parameter. Both deterministic and stochastic schemes allow us to control the direction and speed of the fronts separating spatial domains. The considered stochastic control represents a particular case of noise-sustained front propagation in bistable systems and involves the properties of the optical system under study. In contrast, the proposed deterministic control technique can generally be applied to bistable systems of different natures.

DOI: [10.1103/PhysRevB.108.024307](https://doi.org/10.1103/PhysRevB.108.024307)

I. INTRODUCTION

Besides the well-known Turing patterns, reaction-diffusion systems exhibit a big variety of spatiotemporal dynamics [1–4] including traveling fronts, solitary and periodic pulses, spiral turbulence, scroll waves, and noise-induced pattern formation. In particular, bistable reaction-diffusion media can exhibit dynamics where two different domain types form and evolve in space, creating propagating wave fronts separating both domains. Such propagating wave fronts [5] are a frequent occurrence in chemistry (see, for instance, the Schlögl model [6–8] developed to explain an autocatalytic reaction mechanism), as well as in electronics [9] and flame propagation theory [10], just to name a few.

In the simplest case, front propagation appears in one-dimensional (1D) space. If a bistable medium evolves in 2D space, then the peculiarities of front propagation are additionally determined by the shape of domains formed and enclosed by a particular front. In such a case, one observes an effect often referred to as “coarsening.” Coarsening is a particular form of front propagation and corresponds to the expansion of domains that invade the entire space at the cost of other domains. It is a fundamental phenomenon demonstrated in the context of different areas: physics of liquid crystals [11] and magnetism [12–15], physics and chemistry of materials [16–19], laser physics [20–22], electronics [23], and animal population statistics [24]. It occurs in bistable spatially extended systems [12] and time-delay oscillators [20,21,23] in

situations when a bistable system is prepared in an inhomogeneous state including both steady states. Separating fronts then start to propagate such that growing spatial domains appear and one state (phase) usually begins to dominate the entire extent of the system. It is noteworthy that analogous processes can arise in stochastic systems as an accompaniment of noise-induced phase transitions [25,26].

It is well known that asymmetry of any kind in bistable spatially extended systems has a principal impact on the speed of wave-front propagation, for instance, in bistable reaction-diffusion models [8,27]: The bigger the asymmetry is, the faster wave fronts propagate. Moreover, control over the system’s asymmetry allows one to stop the wave-front propagation or to even invert its direction. In this paper we illustrate these facts by means of numerical modeling of a spatially extended bistable dynamical system describing the optical device considered in Ref. [28]. In particular, we use the Taylor-series techniques to adjust the system’s parameters such that pitchfork and saddle-node bifurcations are created in order to control the system’s asymmetry and consequently to control coarsening. The principal techniques were developed in Ref. [28].

The second strategy for controlling propagating fronts leverages noise [27,29,30]. As previously established, multiplicative noise can influence the systematic part of front dynamics [4,27,31]. We numerically show how this stochastic scheme of propagation control can be implemented in an optical device represented by a stochastic model.

Generally speaking, we consider two options for coarsening control in bistable dynamical systems: deterministic and stochastic approaches. The deterministic control scheme is a

*Corresponding author: semenov.v.v.ssu@gmail.com

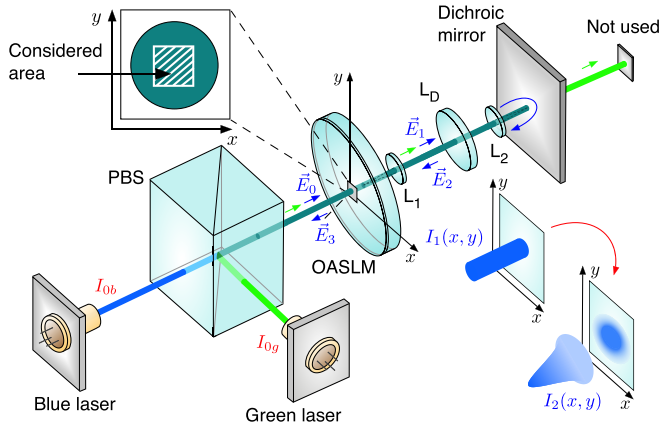


FIG. 1. Single-PS-layer OASLM under simultaneous blue and green illumination when the blue light beam is reflected by the dichroic mirror and creates feedback. The system contains a defocusing lens L_D to emulate local diffusion by spatially broadening the field distribution of the back-reflected optical field. Lenses L_1 and L_2 create $4f$ imaging of the OASLM's state back on itself after reflection by the mirror. PBS, polarizing beam splitter.

universal methodology for approaching the model equation's pitchfork or saddle-node bifurcation normal forms and can hence be applied to dynamical systems of different natures. In contrast, the stochastic approach involves the specificity of the concrete optical device model and hence is strictly speaking not general, though potentially extendable to a wide range of systems governed by similar dynamics. The obtained results complement manifold stochastic phenomena associated with propagating fronts by optical processes and are potentially interesting for specialists in optics, nonlinear dynamics, and the theory of stochastic processes.

II. MODEL UNDER STUDY

The central element of the system discussed in this paper (see Fig. 1) is an optically addressed spatial light modulator (OASLM). Our OASLM model was developed in Ref. [28] based on an experimental characterization of the OASLM fabricated according to the concept reported in Ref. [32]. The OASLM is a light-transmissive device, and it is assumed in the following that the OASLM fully transmits the incident light, i.e., has zero absorption. This is a valid approximation, as the device relies on nanometer-thick photosensitive layers. Such a thin photosensitive layer also means that when considering the interference between different optical fields, one does not need to consider the layer's thickness; it is substantially thinner than the wavelength of any involved optical field. The OASLM operates as an optically controlled birefringent phase plate leveraging a nematic liquid crystal (LC) layer, the phase retardation of which, Γ , is a dynamic quantity. The LC layer is located between two a-As₂S₃ chalcogenide thin films that simultaneously function as photosensitive (PS) and alignment layers. The OASLM is connected to a dc power source resulting in a voltage drop across the LC layer that is considered to be uniform in the absence of spatially structured illumination. However, illumination spatially modifies the PS layers' conductivity, and in turn the local voltage drops across

the LC layer. In response and due to the induced dipole moment, LC molecules change their orientation, which results in a spatial birefringence distribution that is a function of the optical illumination profile. Consequently, an optical wave traversing the LC experiences additional phase retardation Γ between the ordinary and the extraordinary axes and $\Gamma(I) = (\alpha I + \beta)^{-1} + \gamma$ [28]. It is noteworthy that the second PS layer does not increase the device's dynamical complexity and has no principal impact on the dynamics, besides doubling the responsivity of the device [28]. In the rest of this paper we therefore only consider an OASLM with a single PS layer located on the left side of the LC layer.

In our generic setup, schematically illustrated in Fig. 1, the single-PS-layer OASLM operates in the phase modulation regime (the OASLM's rotation angle $\psi = m\pi$, where $m \in \mathbb{Z}$). After traversing the OASLM, a dichroic mirror transmits the green light beam but reflects the blue with reflectivity R , which then interferes with the original blue illumination at the photosensitive layer. Thus the dichroic mirror creates optical feedback and potentially coupling. Generally, optical interference, i.e., a temporal beating originating from the superposition of blue and green light, can be ignored due to the vast difference in the frequencies of the two light sources.

Using Jones matrix calculus, we describe the optical field distributions which determine the system dynamics. Here, we consider uniformly distributed horizontally polarized blue illumination, $\vec{E}_0(x, y) = [E_0, 0]$. After passing the OASLM, one obtains $\vec{E}_1(x, y) = \exp[i(\phi_0 + \Gamma(x, y))]\vec{E}_0(x, y)$, where ϕ_0 is the constant retardation induced by the OASLM without illumination and i is the imaginary unit. The setup in Fig. 1 contains two optical lenses, L_1 and L_2 , to create $4f$ imaging of the OASLM's state back on itself after reflection by the mirror, and a defocusing lens L_D within the optical feedback path. Defocusing leads to blurred imaging, as illustrated in Fig. 1, and its impact can be mathematically described as a convolution with a Gaussian of a width that can be controlled through the positioning lenses. Applying this, one obtains a spatial distribution of the returned-light Jones vector $\vec{E}_2(x, y)$ as

$$\vec{E}_2(x, y) = (R \exp(\phi_1)\vec{E}_1(x, y)) * \left(\frac{1}{2\pi\sigma^2} \exp\left(-\frac{x^2}{2\sigma^2} - \frac{y^2}{2\sigma^2}\right) \right), \quad (1)$$

where ϕ_1 is the retardation accumulated in the external cavity round trip, the asterisk is the convolution operation, and the Gaussian function plays the role of a point spread function widened from the normal imaging setup via the defocusing lens. Finally, the optical wave passes through the OASLM again, and one obtains the field $\vec{E}_3(x, y) = \exp[i(\phi_0 + \Gamma(x, y))]\vec{E}_2(x, y)$, which means that the resulting blue light field at the PS layer on the left side of the OASLM is $\vec{E}_b(x, y) = \vec{E}_0(x, y) + \vec{E}_3(x, y)$ with intensity $I_b(x, y) = |\vec{E}_b(x, y)|^2$. To simplify the model, diffusive processes related to the OASLM are neglected, and the width σ of the optical convolution kernel is chosen to be several times greater than the OASLM resolution, $\sigma_{\text{OASLM}} = 3.5 \mu\text{m}$ (see details in Refs. [28,32]). Finally, optical feedback is considered instantaneous relative to the OASLM's response time ε . The temporal evolution of the blue light's retardation then

takes the form

$$\begin{aligned}\vec{E}_0(x, y) &= \begin{bmatrix} E_0 \\ 0 \end{bmatrix}, \quad \vec{E}_1(x, y) = \exp[i(\phi_0 + \Gamma(x, y))] \begin{bmatrix} E_0 \\ 0 \end{bmatrix}, \\ \vec{E}_2(x, y) &= (R \exp(\phi_1) \vec{E}_1(x, y)) * \left(\frac{1}{2\pi\sigma^2} \exp\left(-\frac{x^2}{2\sigma^2} - \frac{y^2}{2\sigma^2}\right) \right), \\ \vec{E}_3(x, y) &= \exp[i(\phi_0 + \Gamma(x, y))] \vec{E}_2(x, y), \quad I_b(x, y) = |\vec{E}_0(x, y) + \vec{E}_3(x, y)|^2, \\ \varepsilon \frac{d\Gamma(x, y)}{dt} &= -\Gamma(x, y) + \frac{1}{\alpha_b I_b(x, y) + \tilde{\alpha}_g I_{0g} + \beta} + \gamma,\end{aligned}\quad (2)$$

where $\tilde{\alpha}_g = \frac{\lambda_g}{\lambda_b} \alpha_g$ is the retardation effect of green light intensity I_{0g} on the blue signal.

If one neglects spatial aspects of the dynamics and excludes the optical convolution implemented by L_D , the system is reduced to an ordinary differential equation (see Ref. [28]) for the temporal evolution of the retardation:

$$\begin{aligned}\varepsilon \frac{d\Gamma}{dt} &= -\Gamma + \frac{1}{\alpha_b I_b(\Gamma) + \tilde{\alpha}_g I_{0g} + \beta} + \gamma, \\ I_b(\Gamma) &= I_{0b} \{1 + R^2 + 2R \cos(2\phi_0 + \phi_1 + 2\Gamma)\}.\end{aligned}\quad (3)$$

The action of the convolution operation in the spatially extended model (2) is associated with homogenous coupling of the system state at any point on the (x, y) plane with its neighbor states in some range $x \in [x - \Delta x; x + \Delta x]$, $y \in [y - \Delta y; y + \Delta y]$. Defocusing represents a natural physical approach for the homogeneous coupling implementation similar to diffusive effects occurring inside the OASLM. If the coupling radius does not exceed the OASLM's linear pixel size, one deals with local coupling. Then, one can expect to observe the effects of wave propagation and coarsening in Eq. (2), where the system parameters correspond to the regime of bistability in the single oscillator of Eq. (3). Our numerical study is based on modeling Eq. (2) using the Heun method [33] with time step $\Delta t = 10^{-3}$. In the rest of this paper, Eqs. (2) are studied for the fixed parameter set $R = 0.95$, $\alpha_b = 0.117 \text{ m}^2 \text{ rad}^{-1} \text{ W}^{-1}$, $\alpha_g = 98.5 \times 10^{-6} \text{ m}^2 \text{ rad}^{-1} \text{ W}^{-1}$, $\beta = 0.052 \text{ rad}^{-1}$, $\gamma = -0.55 \text{ rad}$, $\phi_0 = \pi/2 \text{ rad}$, $\phi_1 = \pi \text{ rad}$, $\varepsilon = 1 \text{ s}$, and $\sigma = 10^{-5} \text{ m}$ and varying I_{0b} and I_{0g} . The blue and green light wavelengths are chosen according to experiments carried out in Ref. [28]: $\lambda_b = 450 \times 10^{-9} \text{ m}$ and $\lambda_g = 532 \times 10^{-9} \text{ m}$, correspondingly.

III. DETERMINISTIC CONTROL

As demonstrated in Ref. [28], one can implement the pitchfork and the saddle-node bifurcation of steady states in our system described by Eq. (3), if I_{0b} and I_{0g} are chosen according to the corresponding bifurcation condition curves depicted in Fig. 2. In more detail, when I_{0b} and I_{0g} are varied according to the curves in Fig. 2, the right-hand-side function $f(\Gamma)$ of Eq. (3) represented in the form $\frac{d\Gamma}{dt} = f(\Gamma)$ evolves in some range of Γ as a cubic function and a quadratic function. Then Eq. (3) is considered as the pitchfork and saddle-node bifurcation normal forms, $\frac{d\Gamma}{dt} = b\Gamma - d\Gamma^3$ and $\frac{d\Gamma}{dt} = a + c\Gamma^2$. Here, we use these bifurcation conditions to control the effect of coarsening in Eq. (2). We consider Eq. (3) in the form

$\frac{d\Gamma}{dt} = f(\Gamma)$ and illustrate the right-hand-side function $f(\Gamma)$ for varying I_{0b} and I_{0g} . For all parameter values, $f(\Gamma)$ shows three steady states corresponding to the condition $f(\Gamma) = 0$: stable steady states A and B and an unstable equilibrium between them (see Figs. 3 and 4). We visualize the fact that the symmetry properties of Eq. (3) describing the local dynamics without coupling are reflected in the duration and direction of coarsening in Eq. (2). For this purpose, we fix the initial spatial pattern at $t = 0$ and observe the spatial evolution when I_{0b} and I_{0g} change.

A. Pitchfork bifurcation conditions

Let us fix light intensities $I_{0g} = 22 \text{ W/m}^2$ and $I_{0b} = |\vec{E}_0|^2 = 0.015 \text{ W/m}^2$ in Eq. (2). This parameter set corresponds to the regime of bistability in the single-oscillator model described by Eq. (3); however, the pitchfork bifurcation conditions are not fulfilled [this parameter set corresponds to point 1 in Fig. 2(a)], and the right-hand-side function of Eq. (3) is asymmetric [see Fig. 3(a)]. In that case, the spatially extended model described by Eq. (2) exhibits coarsening; see Figs. 3(b1)–3(b3). The system asymmetry is reflected in the fact that the basin of attraction of state B is larger than that of state A, and the unstable fixed point is closer to attractor A than to the stable steady state B. This results in the spatial evolution of Eq. (2) such that the red domains corresponding to state B extend and invade the entire space (x, y) .

Increasing I_{0g} allows us to fulfill the pitchfork bifurcation conditions at $I_{0g} \approx 30.1 \text{ W/m}^2$ [point 2 in Fig. 2(a)], for

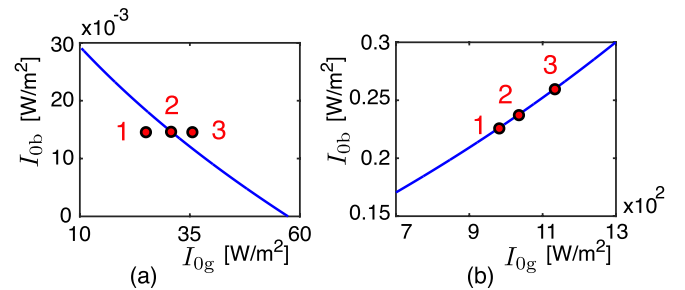


FIG. 2. Pitchfork (a) and saddle-node (b) bifurcation condition curves for varying I_{0b} and I_{0g} in Eq. (3) (see Ref. [28] for details). System parameters are as follows: $\varepsilon = 1 \text{ s}$, $\alpha_b = 0.117 \text{ m}^2 \text{ rad}^{-1} \text{ W}^{-1}$, $\alpha_g = 98.5 \times 10^{-6} \text{ m}^2 \text{ rad}^{-1} \text{ W}^{-1}$, $\beta = 0.052 \text{ rad}^{-1}$, $\gamma = -0.55 \text{ rad}$, $\phi_0 = \pi/2 \text{ rad}$, $\phi_1 = \pi \text{ rad}$, $\lambda_b = 450 \times 10^{-9} \text{ m}$, $\lambda_g = 532 \times 10^{-9} \text{ m}$, and $R = 0.95$.

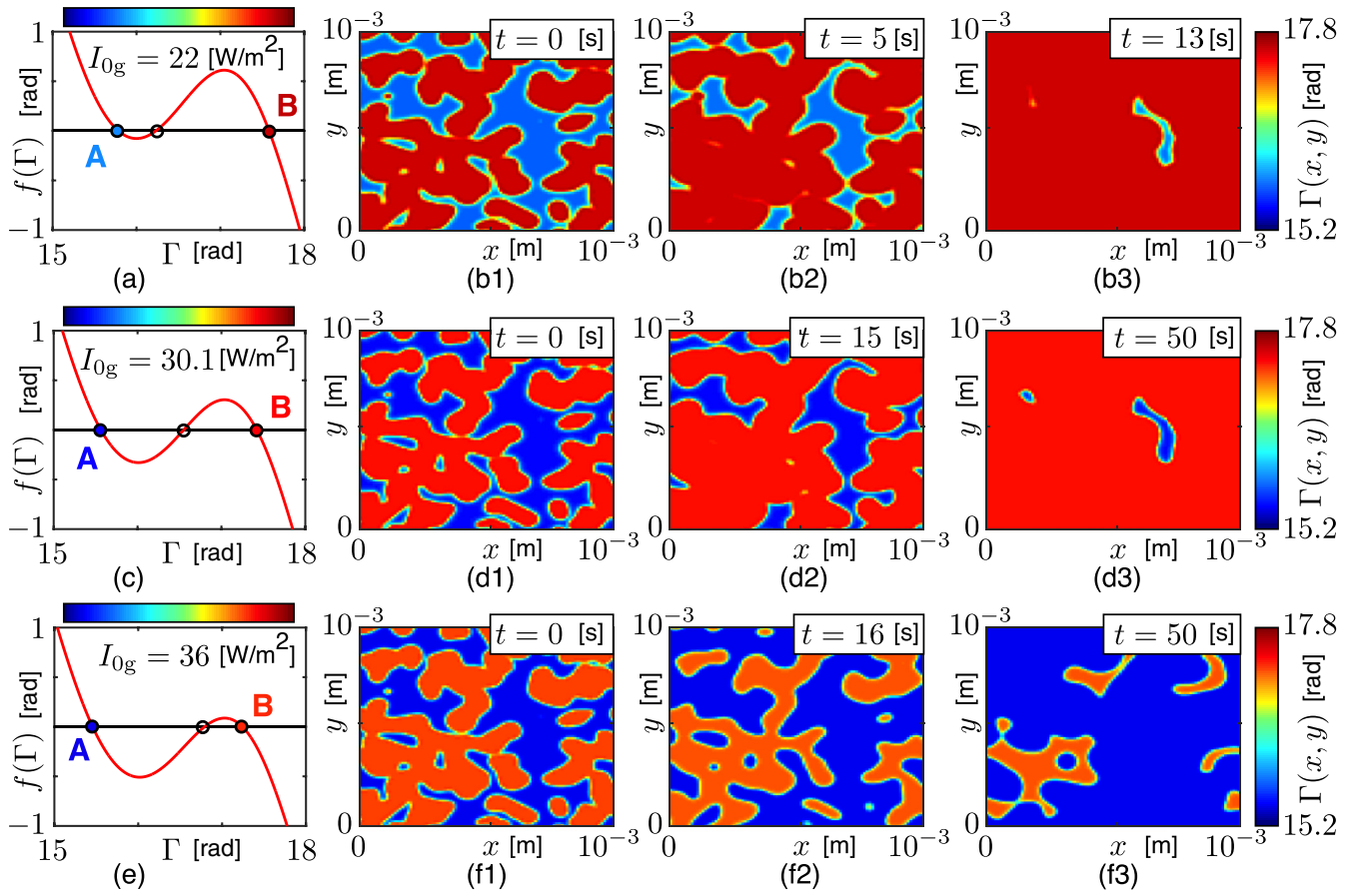


FIG. 3. Coarsening and the pitchfork bifurcation conditions: evolution of the right-hand-side function of Eq. (3) and coarsening in Eq. (2) for increasing green light intensity: $I_{0g} = 22 \text{ W/m}^2$ [(a) and (b1)–(b3)] corresponding to point 1 in Fig. 2(a), $I_{0g} = 30.1 \text{ W/m}^2$ [(c) and (d1)–(d3)] corresponding to point 2 in Fig. 2(a), and $I_{0g} = 36 \text{ W/m}^2$ [(e) and (f1)–(f3)] corresponding to point 3 in Fig. 2(a). Other parameters are as follows: $\varepsilon = 1 \text{ s}$, $\alpha_b = 0.117 \text{ m}^2 \text{ rad}^{-1} \text{ W}^{-1}$, $\alpha_g = 98.5 \times 10^{-6} \text{ m}^2 \text{ rad}^{-1} \text{ W}^{-1}$, $\beta = 0.052$, $\gamma = -0.55 \text{ rad}$, $\phi_0 = \pi/2 \text{ rad}$, $\phi_1 = \pi \text{ rad}$, $\lambda_b = 450 \times 10^{-9} \text{ m}$, $\lambda_g = 532 \times 10^{-9} \text{ m}$, $R = 0.95$, $I_{0b} = 0.01506 \text{ W/m}^2$, and $\sigma = 10^{-5} \text{ m}$.

which the asymmetry of the right-hand-side function $f(\Gamma)$ is minimized [see Fig. 3(c)], and coarsening is substantially slower. Consequently, a longer time is necessary for the transformation of the same initial metastable state as in Fig. 3(b1) [the initial states in Figs. 3(b1), 3(d1), and 3(f1) are identical] into the quiescent regime when either steady state A or B invades the entire space; see Figs. 3(d1)–3(d3). It should be noted that in the case of minimal asymmetry, the probabilities to observe the final state $\Gamma(x, y) = A$ or $\Gamma(x, y) = B$ starting from random initial conditions are almost identical.

If one continues to increase the green light intensity, the phase space structure is inverted in comparison with the initial configuration, as can be seen from comparison of $f(\Gamma)$ in Figs. 3(a) and 3(e). The motion of fronts separating domains reverses, and the coarsening direction becomes the opposite: Steady state A invades the whole space; see Figs. 3(f1)–3(f3) corresponding to $I_{0b} = 0.015 \text{ W/m}^2$ and $I_{0g} = 36 \text{ W/m}^2$ [point 3 in Fig. 2(a)].

B. Saddle-node bifurcation conditions

Varying I_{0b} and I_{0g} according to the curve obtained using the saddle-node bifurcation conditions, corresponding to the blue line in Fig. 2(b), allows us to move the right-hand-side function of Eq. (3) up and down; see Figs. 4(a), 4(c), and 4(e).

A symmetric configuration of $f(\Gamma)$ can be achieved during this motion [see Fig. 4(c)], and the same effects as in the previous section can be observed. First, the system's asymmetry is well pronounced, as illustrated in Fig. 4(a), and state B rapidly invades the space (x, y) ; see Figs. 4(b1)–4(b3). When I_{0b} and I_{0g} are adjusted such that the saddle-node bifurcation conditions are fulfilled, the system passes through the symmetric state [see Fig. 4(c)], and the coarsening effect slows down as illustrated in Figs. 4(d1)–4(d3). Further changing I_{0b} and I_{0g} inverts the asymmetry [see Fig. 4(e)], and the motion of fronts separating blue and red domains reverses its direction [see Figs. 4(f1)–4(f3)].

IV. STOCHASTIC CONTROL

Consider a stochastic model of the optical setup illustrated in Fig. 1. For that purpose, it is assumed that the green light illumination contains a stochastic contribution according to $I_{0g}(x, y) = I_{0g} + \xi(x, y)$. Here, $\xi(x, y)$ represents a source of spatial colored noise described by the first-order Ornstein-Uhlenbeck process

$$\tau_c \frac{d\xi(x, y)}{dt} = -\xi(x, y) + \sqrt{2D_g \tau_c} n(x, y, t), \quad (4)$$

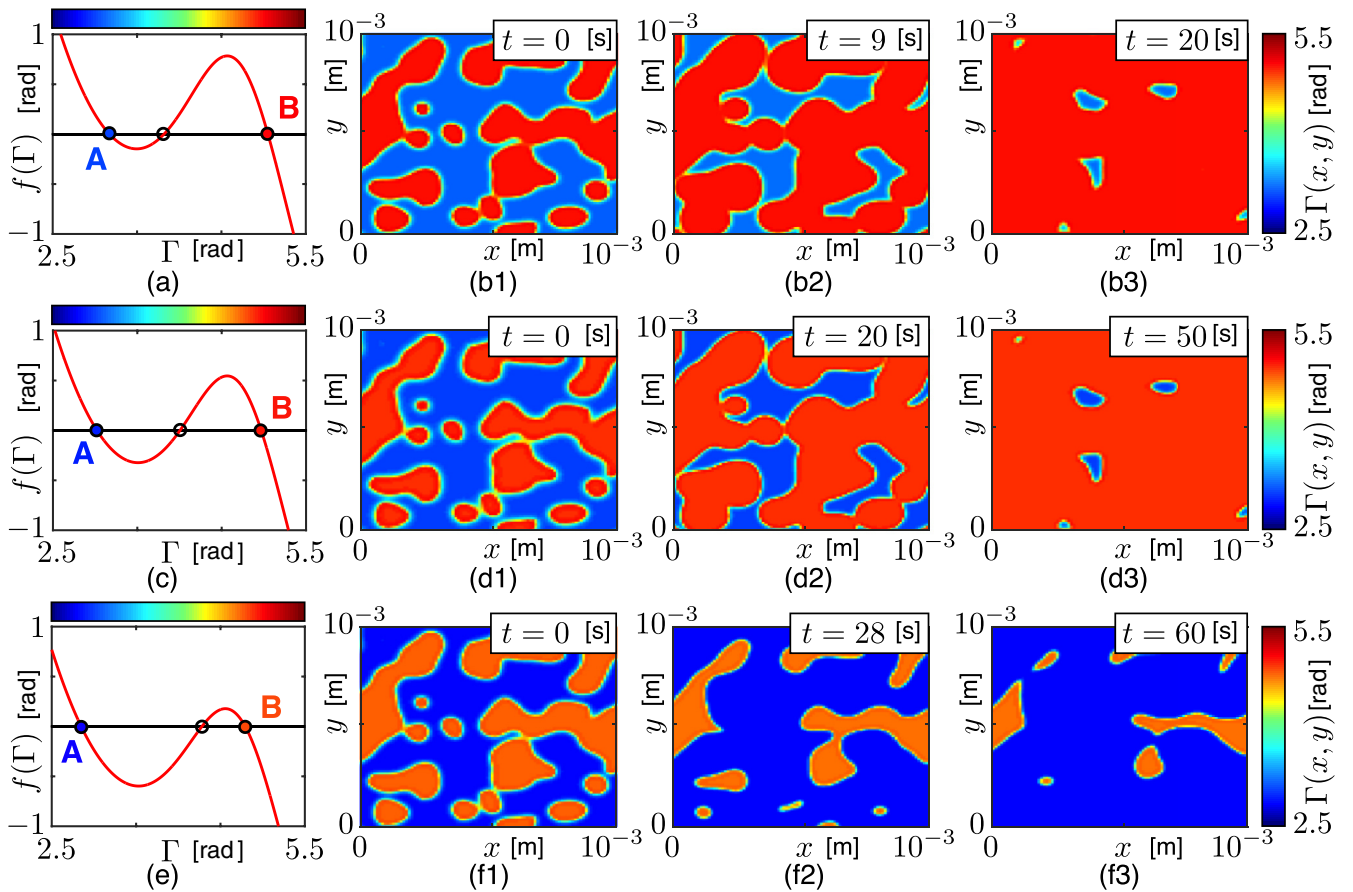


FIG. 4. Coarsening and the saddle-node bifurcation conditions: evolution of the right-hand-side function of Eq. (3) and coarsening in Eq. (2) when I_{0b} and I_{0g} vary according to the saddle-node bifurcation conditions for Eq. (3): $I_{0b} = 0.228 \text{ W/m}^2$ and $I_{0g} = 990 \text{ W/m}^2$ [(a) and (b1)–(b3)] corresponding to point 1 in Fig. 2(b), $I_{0b} = 0.241 \text{ W/m}^2$ and $I_{0g} = 1050 \text{ W/m}^2$ [(c) and (d1)–(d3)] corresponding to point 2 in Fig. 2(b), and $I_{0b} = 0.2645 \text{ W/m}^2$ and $I_{0g} = 1153 \text{ W/m}^2$ [(e) and (f1)–(f3)] corresponding to point 3 in Fig. 2(b). Other parameters are as follows: $\varepsilon = 1 \text{ s}$, $\alpha_b = 0.117 \text{ m}^2 \text{ rad}^{-1} \text{ W}^{-1}$, $\alpha_g = 98.5 \times 10^{-6} \text{ m}^2 \text{ rad}^{-1} \text{ W}^{-1}$, $\beta = 0.052 \text{ rad}^{-1}$, $\gamma = -0.55 \text{ rad}$, $\phi_0 = \pi/2 \text{ rad}$, $\phi_1 = \pi \text{ rad}$, $\lambda_b = 450 \times 10^{-9} \text{ m}$, $\lambda_g = 532 \times 10^{-9} \text{ m}$, $R = 0.95$, and $\sigma = 10^{-5} \text{ m}$.

where τ_c is the colored noise correlation time, $n(x, y, t)$ is a normalized source of white Gaussian noise, and D_g plays the role of the noise intensity. The temporal and spatial correlation properties of the noise source $n(x, y, t)$ at any point \vec{r}_0 are described by the delta function: $\langle n(\vec{r}_0, t) \rangle = 0$, $\langle n(\vec{r}_0, t)n(\vec{r}_0, t + \tau) \rangle = \delta(\tau)$, and $\langle n(\vec{r}_0, t)n(\vec{r}_0 + \vec{r}_d, t) \rangle = \delta(\vec{r}_d)$ (here, the brackets $\langle \cdot \rangle$ denote the mean value), which means that the correlation time of the source $n(x, y, t)$ equals zero and the noise signal values $n(x, y, t)$ at any two points (x_1, y_1) and (x_2, y_2) are statistically independent.

Physically, the random spatial component $\xi(x, y)$ can be included in the green illumination by adding an electronically addressed spatial light modulator that spatially modifies the green illumination. In such colored noise, the spatially random illumination is characterized by a finite temporal correlation determined by the parameter τ_c . It is assumed in the following that the noise correlation time τ_c is much shorter than the OASLM's response time ε .

Since the term $I_{0g} + \xi(x, y)$ describes a light intensity, it cannot be negative. To account for this, the green light intensity is introduced into the model as $k(I_{0g} + \xi(x, y))$, where $k = 1$ for $I_{0g} + \xi(x, y) \geq 0$ and $k = 0$ otherwise. Finally, the

stochastic spatial model of the setup in Fig. 1 takes the form

$$\begin{aligned} \varepsilon \frac{d\Gamma(x, y)}{dt} &= -\Gamma(x, y) \\ &+ \frac{1}{\alpha_b I_b(x, y) + \tilde{\alpha}_g k(I_{0g} + \xi(x, y)) + \beta} + \gamma, \\ \tau_c \frac{d\xi(x, y)}{dt} &= -\xi(x, y) + \sqrt{2D_g \tau_c} n(x, y, t), \\ k &= \begin{cases} 1, & I_{0g} + \xi(x, y) \geq 0 \\ 0, & I_{0g} + \xi(x, y) < 0, \end{cases} \end{aligned} \quad (5)$$

where all the Jones vector components determining the blue light intensity are the same as in Eq. (2).

First, Eq. (5) is considered for a set of parameters corresponding to Fig. 3(a) when the basin of attraction of steady state B is larger than the basin of state A. Equation (5) therefore exhibits coarsening, and the system state $\Gamma(x, y) = B$ invades the entire space in the absence of noise, $D_g = 0$ [see Figs. 5(a)–5(c)]. However, increasing noise intensity D_g slows down the effect of coarsening [see Figs. 5(d)–5(f)], and

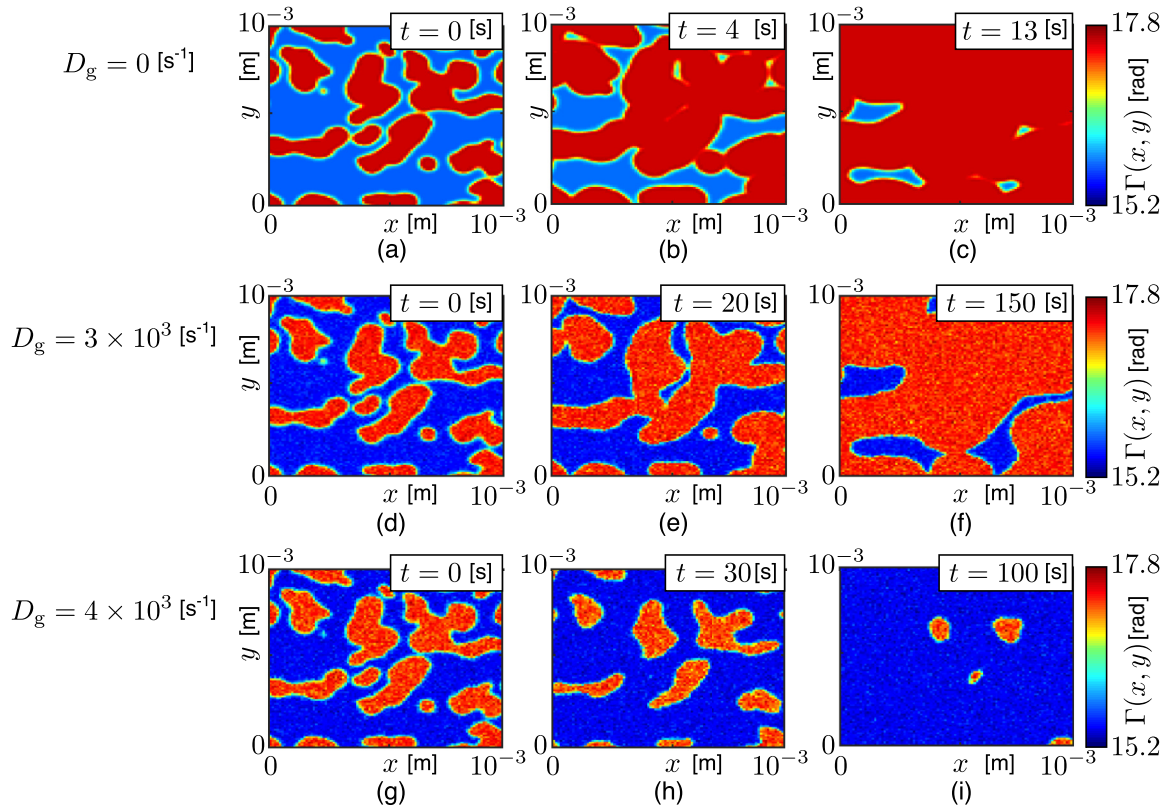


FIG. 5. Coarsening in Eq. (5) for increasing noise intensity: $D_g = 0$ [(a)–(c)], $D_g = 3 \times 10^3$ [(d)–(f)], and $D_g = 4 \times 10^3$ [(g)–(i)]. Other parameters are as follows: $\varepsilon = 1$ s, $\alpha_b = 0.117$ m² rad⁻¹ W⁻¹, $\alpha_g = 98.5 \times 10^{-6}$ m² rad⁻¹ W⁻¹, $\beta = 0.052$ rad⁻¹, $\gamma = -0.55$ rad, $\phi_0 = \pi/2$ rad, $\phi_1 = \pi$ rad, $\lambda_b = 450 \times 10^{-9}$ m, $\lambda_g = 532 \times 10^{-9}$ m, $R = 0.95$, $I_{0b} = |\vec{E}_0|^2 = 0.01506$ W/m², $I_{0g} = 22$ W/m², $\sigma = 10^{-5}$ m, and $\tau_c = 0.01$ s.

above a threshold at around $D_g \approx 3.7 \times 10^3$ s⁻¹, noise inverts the front propagation dynamics and state A dominates [see Figs. 5(g)–5(i)].

Similarly, if the system parameter set corresponds to Fig. 3(e), one observes invading state A [Figs. 6(a)–6(c)].

In such a case, increasing the noise intensity speeds up the process [Figs. 6(d)–6(f)]. Thus it is demonstrated in Figs. 5 and 6 that, depending on the particular system configuration, noise can speed up coarsening, slow it down, or even invert the direction.

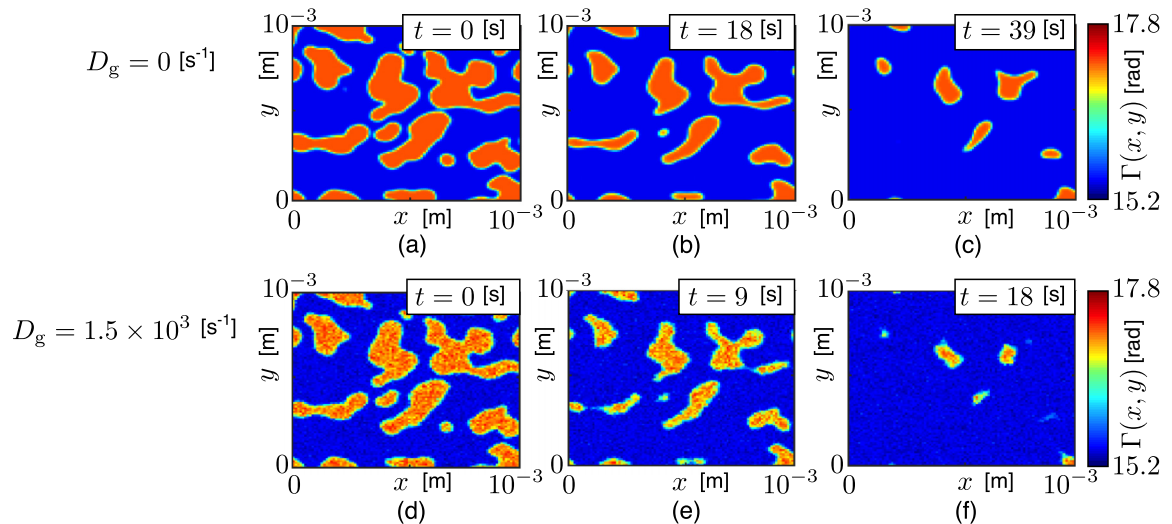


FIG. 6. Coarsening in Eq. (5) for increasing noise intensity: $D_g = 0$ [(a)–(c)] and $D_g = 1.5 \times 10^3$ [(d)–(f)]. Other parameters are as follows: $\varepsilon = 1$ s, $\alpha_b = 0.117$ m² rad⁻¹ W⁻¹, $\alpha_g = 98.5 \times 10^{-6}$ m² rad⁻¹ W⁻¹, $\beta = 0.052$ rad⁻¹, $\gamma = -0.55$ rad, $\phi_0 = \pi/2$ rad, $\phi_1 = \pi$ rad, $\lambda_b = 450 \times 10^{-9}$ m, $\lambda_g = 532 \times 10^{-9}$ m, $R = 0.95$, $I_{0b} = |\vec{E}_0|^2 = 0.01506$ W/m², $I_{0g} = 36$ W/m², $\sigma = 10^{-5}$ m, and $\tau_c = 0.01$ s.

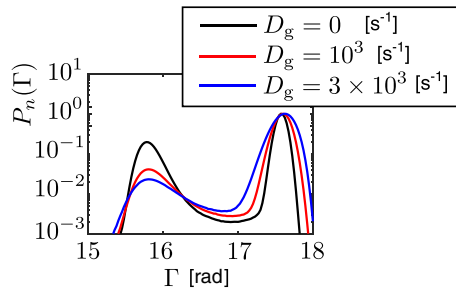


FIG. 7. Evolution of the normalized probability density function $P_n(\Gamma)$ caused by the varying noise intensity D_g in Eq. (6). Parameters are as follows: $\varepsilon = 1$ s, $\alpha_b = 0.117$ m² rad⁻¹ W⁻¹, $\alpha_g = 98.5 \times 10^{-6}$ m² rad⁻¹ W⁻¹, $\beta = 0.052$ rad⁻¹, $\gamma = -0.55$ rad, $\phi_0 = \pi/2$ rad, $\phi_1 = \pi$ rad, $\lambda_b = 450 \times 10^{-9}$ m, $\lambda_g = 532 \times 10^{-9}$ m, $R = 0.95$, $I_{ob} = 0.01506$ W/m², $I_{og} = 22$ W/m², and $\tau_c = 0.01$ s.

The theoretically rigorous explanation of the stochastic coarsening control in OASLM-based spatial models is significantly more challenging as compared with, for instance, the theoretical analysis given in Refs. [4,31] for basic reaction-diffusion models with multiplicative noise. In particular, the “small-noise-expansion approach” used in Refs. [4,31] cannot be applied in the context of Eq. (5) due to the fact that any polynomial expression of Eq. (5) is challenging to obtain and will furthermore give rise to stochastic terms in all the polynomial components. Consequently, it becomes extremely challenging to distinguish the systematic part of the noise influence. Nevertheless, we would like to emphasize the similarity between the processes observed in the basic models discussed in Refs. [4,27,31] and in the OASLM-based spatial model described by Eq. (5). To visualize the fact that stochastic forcing has an asymmetric impact on Eq. (5), a single-oscillator stochastic model corresponding to Eq. (5) at $\sigma \rightarrow 0$ is taken into consideration. If $\sigma \rightarrow 0$, the spatial coupling is absent, and the retardation Γ individually evolves according to Eq. (3) at each point of the illuminated area, but in the presence of the noise term ξ

$$\begin{aligned} \varepsilon \frac{d\Gamma}{dt} &= -\Gamma + \frac{1}{\alpha_b I_b + \tilde{\alpha}_g (I_{og} + \xi) + \beta} \\ &\quad + \gamma + \sqrt{0.02} n_d(t), \\ \tau_c \frac{d\xi}{dt} &= -\xi + \sqrt{2D_g \tau_c} n(t), \\ I_b &= I_{ob} \{1 + R^2 + 2R \cos(2\phi_0 + \phi_1 + 2\Gamma)\}, \end{aligned} \quad (6)$$

where the additive white Gaussian noise term $\sqrt{0.02} n_d(t)$ has no impact on the system’s symmetry and is included to obtain a stationary distribution of the normalized probability density function for the dynamical variable, $P_n(\Gamma)$, in numerical simulations (transitions between two steady states are very rare without additive noise). The evolution of $P_n(\Gamma)$ caused by increasing noise intensity D_g illustrated in Fig. 7 indicates that the left peak becomes broadened faster than the right one. Thus the action of noise $\xi(t)$ is significantly stronger in the vicinity of the left steady state $\Gamma_* = A$. This effect is similar to the noise-induced evolution of $P_n(u)$ in the phenomenological

model defined by the equation $\frac{dx}{dt} = -x(x - a + \xi_a)(x + b + \xi_b) + \nabla^2 x$ (see Ref. [27]).

V. CONCLUSIONS

The peculiarities of the bifurcation transitions to the bistable dynamics discussed in Ref. [28] in the context of single-oscillator models are reflected in the behavior of the corresponding spatially extended systems, as, for example, in Eq. (2) or similar models corresponding to different OASLM rotation angles or incident light polarization states, as formation of localized spatial domains corresponding to the attraction of two coexisting steady states. If the right-hand-side function is asymmetric, the steady state characterized by the larger basin of attraction invades the entire space. This process is accompanied by the effect of coarsening, which is determined by both asymmetry and the shape of evolving domains.

In the proposed model, the spatial coupling is introduced as the result of Gaussian blurring mathematically described by a convolution with a Gaussian of a controllable width. Physically, it can be implemented in different ways. A trivial way to include such Gaussian blurring, i.e., diffusion, in the optical feedback would be to slightly align imaging of the optical feedback out of focus relative to the position of the OASLM. A second, potentially cleaner approach would be using a $4f$ correlator with a tunable spatial filtering functionality. Such a $4f$ correlator uses multiplication in Fourier space, which corresponds to convolution in real space. Hence implementing a Gaussian intensity function, for example, with an electrically controlled spatial light modulator, in the Fourier space corresponds to the convolution of the original Gaussian of the imaging setup with the Gaussian of the spatial filtering. As a consequence, the optical feedback would have the Gaussian width $w_{FB} = \sqrt{w_O^2 + w_{SF}^2}$, where w_O is the Abbe resolution of the optical imaging setup and w_{SF} is the width of the Gaussian filter defined by the $4f$ correlator.

Applying the saddle-node or pitchfork bifurcation conditions, one can remove the system asymmetry, and then the dominating domain expansion is slowed down. Moreover, if the incident green and blue light intensities vary and obey the saddle-node bifurcation condition, one can controllably invert the front propagation direction. However, the saddle-node bifurcation conditions do not allow us to rigorously define the absolutely symmetric state, while applying the pitchfork bifurcation conditions provides for mathematical derivation of appropriate parameter values.

The second approach to control coarsening is the introduction of noise into the system. In particular, the presence of parametric noise modulating the green light intensity gives rise to speeding up or slowing down and inverting the effects of front propagation and coarsening. The ability to control the dynamics by increasing the noise intensity strength results from the fact that fluctuation growth changes the system symmetry. Detailed theoretical analysis of the stochastic control represents an issue for further investigations.

In this paper we focused on wave fronts and coarsening, whereas other phenomena that are typical for bistable

extended systems, such as stochastic resonance [34], critical phase transitions [35], and related issues, were not considered. We also plan to consider such effects in the context of the symmetry control in further studies.

The interdisciplinary significance of the obtained results consists in the developed approach for the control of propagating fronts in bistable spatially extended systems of any nature exhibiting the coexistence of two steady states. Representing the function that is responsible for the local dynamics in a polynomial form by using the Taylor-series expansion, one can derive the pitchfork or saddle-node bifurcation conditions in a similar way to that pursued in this paper and then apply them to tune the system symmetry and, resultantly, the front propagation speed and direction. Finally, the developed approach for controlling the symmetry of bistable spatially extended systems offers

great opportunities for future implementations of spin-state networks.

The data that support the findings of this study are available from the corresponding author upon reasonable request.

ACKNOWLEDGMENTS

We are very grateful to Prof. Serhiy Yanchuk for fruitful discussions. This work has been supported by the EIPHI Graduate School (Contract No. ANR-17-EURE-0002) and the Bourgogne-Franche-Comté Region and H2020 Marie Skłodowska-Curie Actions (MULTIPLY, No. 713694). The results of the numerical simulations presented in Secs. III and IV were obtained by V.V.S. in the framework of project 22-72-00038 supported by Russian Science Foundation.

The authors have no conflicts to disclose.

-
- [1] Y. Kuramoto, *Chemical Oscillations, Waves and Turbulence* (Springer-Verlag, Berlin, 1984).
- [2] A. Mikhailov, *Foundations of Synergetics I: Distributed Active Systems* (Springer-Verlag, New York, 1990).
- [3] R. Kapral and K. Showalter, *Chemical Waves and Patterns* (Kluwer, Dordrecht, 1995).
- [4] J. Garcia-Ojalvo and J. Sancho, *Noise in Spatially Extended Systems* (Springer, New York, 1999).
- [5] It is important to note that the term “wave front” does not refer to the surface over which an optical wave has a constant phase. Here, a wave front or simply a front refers to the context of, for example, fluid dynamics and describes a boundary between domains corresponding to different quiescent steady-state regimes in bistable reaction-diffusion systems.
- [6] F. Schlögl, *Z. Phys.* **253**, 147 (1972).
- [7] F. Schlögl, C. Escher, and R. Berry, *Phys. Rev. A* **27**, 2698 (1983).
- [8] J. Löber, R. Coles, J. Siebert, H. Engel, and E. Schöll, in *Engineering of Chemical Complexity II*, edited by A. Mikhailov and G. Ertl (World Scientific, Singapore, 2014), Chap. 11, pp. 185–207.
- [9] E. Schöll, *Nonlinear Spatio-Temporal Dynamics and Chaos in Semiconductors*, Nonlinear Science Series Vol. 10 (Cambridge University Press, Cambridge, 2001).
- [10] Y. Zel’dovich and D. Frank-Kamenetskii, *Dokl. Akad. Nauk SSSR* **19**, 693 (1938).
- [11] B. Yurke, A. Pagellis, I. Chuang, and N. Turok, *Physica B (Amsterdam)* **178**, 56 (1992).
- [12] A. Bray, *Adv. Phys.* **43**, 357 (1994).
- [13] L. Cugliandolo, *Physica A (Amsterdam)* **389**, 4360 (2010).
- [14] F. Caccioli, S. Franz, and M. Marsili, *J. Stat. Mech.: Theory Exp.* (2008) P07006.
- [15] J. Denholm and S. Redner, *Phys. Rev. E* **99**, 062142 (2019).
- [16] Y. Goh and R. Jacobs, *New J. Phys.* **4**, 81 (2002).
- [17] C. Zhang, L. Yu, and H. Wang, *Materials* **12**, 2096 (2019).
- [18] L. Zhang, Q. Liu, and P. Crozier, *J. Mater. Chem. A* **7**, 11756 (2019).
- [19] P. Geslin, M. Buchet, T. Wada, and H. Kato, *Phys. Rev. Mater.* **3**, 083401 (2019).
- [20] G. Giacomelli, F. Marino, M. Zaks, and S. Yanchuk, *Europhys. Lett.* **99**, 58005 (2012).
- [21] F. Marino, G. Giacomelli, and S. Barland, *Phys. Rev. Lett.* **112**, 103901 (2014).
- [22] J. Javaloyes, T. Ackemann, and A. Hurtado, *Phys. Rev. Lett.* **115**, 203901 (2015).
- [23] V. Semenov and Y. Maistrenko, *Chaos* **28**, 101103 (2018).
- [24] U. Dobramysl, M. Mobilia, M. Pleimling, and U. Täuber, *J. Phys. A* **51**, 063001 (2018).
- [25] C. Van den Broeck, *Phys. Rev. E* **55**, 4084 (1997).
- [26] O. Carrillo, M. Ibañes, J. García-Ojalvo, J. Casademunt, and J. Sancho, *Phys. Rev. E* **67**, 046110 (2003).
- [27] A. Engel, *Phys. Lett. A* **113**, 139 (1985).
- [28] V. Semenov, X. Porte, I. Abdulhalim, L. Larger, and D. Brunner, *Chaos* **31**, 121104 (2021).
- [29] L. Schimansky-Geier, A. Mikhailov, and W. Ebeling, *Ann. Phys. (Berlin)* **495**, 277 (1983).
- [30] M. Löcher, D. Cigna, and E. Hunt, *Phys. Rev. Lett.* **80**, 5212 (1998).
- [31] V. Méndez, I. Llopis, D. Campos, and W. Horsthemke, *J. Theor. Biol.* **281**, 31 (2011).
- [32] M. Kirzhner, M. Klebanov, V. Lyubin, N. Collings, and I. Abdulhalim, *Opt. Lett.* **39**, 2048 (2014).
- [33] R. Mannella, *Int. J. Mod. Phys. C* **13**, 1177 (2002).
- [34] L. Gammaitoni, P. Hänggi, P. Jung, and F. Marchesoni, *Rev. Mod. Phys.* **70**, 223 (1998).
- [35] M. Faggian, F. Ginelli, F. Marino, and G. Giacomelli, *Phys. Rev. Lett.* **120**, 173901 (2018).